J Electroceram (2011) 27:56–65
DOI 10.1007/s10832-011-9650-y

Influence of substitution on dielectric diffuseness in $Ba_{(1-x)}Bi_{(2+2x/3)}Nb_2O_9$ ceramics prepared by chemical precursor decomposition method

Debasis Dhak · Prasanta Dhak · Panchanan Pramanik

Received: 18 January 2011 / Accepted: 1 August 2011 / Published online: 20 August 2011

Abstract Barium bismuth niobate, $Ba_{(1-x)}Bi_{(2+2x/3)}Nb_2O_9$ (BBN with x=0.0, 0.1, 0.2, 0.3, 0.4) ceramic powders in the nanometer range were prepared by chemical precursor decomposition method (CPD). The single phase layered perovskite was prepared throughout the composition range studied. No intermediate phase was found during heat treatment at and above 600°C. The crystallite size and the particle size, obtained from XRD and TEM respectively, were in the range of 15–30 nm. The addition of Bi_2O_3 substantially improved the sinterability associated with high density (96%) which was otherwise difficult in the case of pure $BaBi_2Nb_2O_9$ (BBN x=0.0). The sintering was done at 900°C for 4 h. The relative permittivity of BBN ceramics at both room temperature and in the vicinity of the temperature of maximum permittivity (T_m) has increased significantly with increase in bismuth content and loss is also decreased to a certain level of bismuth doping. T_m increased with increase in Bi_2O_3. The diffuseness (γ) in the phase transition was found to increase from 1.54 to 1.98 with the increase in Ba^{2+} substitution level from x=0.0 to x=0.3.

Keywords Ceramics · Chemical synthesis · Dielectric properties

D. Dhak (✉)
Department of Chemistry, Serampore College,
Serampore 712201, Hooghly, India
e-mail: debasisdhak@yahoo.co.in

P. Dhak · P. Pramanik
Department of Chemistry,
Indian Institute of Technology Kharagpur,
Kharagpur 721302, India

P. Dhak (✉)
Department of Chemistry, Jadavpur University,
Kolkata 700032, India
e-mail: pdhak_chem@yahoo.com

1 Introduction

The interest in Bi-based layer-structured ferroelectric oxides (BLSF) has been raised during the last decade since these materials have high polarization fatigue resistance, and is able to withstand 10^{12} erase/rewrite operations [1–5]. The crystal structure and chemical composition of these layered perovskites were systematically studied by Aurivillius [3] in the 1950's with a general formula of $(Bi_2O_2)^{2+}(A_{m-1}B_mO_{3m+1})^{2-}$, consisting of m-perovskite units sandwiched between bismuth oxide layers called the family of bismuth layered structured ferroelectrics (BLSFs) [6], where A and B are the two types of cations that enter the perovskite unit. A is Bi^{3+}, Ba^{2+}, Sr^{2+}, Pb^{2+}or K^{1+}; B is Ti^{4+}, Ta^{5+}, Nb^{5+}, Mo^{6+} or W^{6+} and m=1, 2, 3, 4, 5, 6 [7]. The oxygen octahedral blocks responsible for ferroelectric behavior are interleaved with $(Bi_2O_2)^{2+}$ layers resulting in a highly anisotropic crystallographic structure where the 'c' parameter [normal to $(Bi_2O_2)^{2+}$ layers] is much greater than 'a' and 'b' parameters of the orthorhombic cell. Besides that, the Bi-layered perovskites demonostrate highly anisotropic electrical properties [8].

In the beginning of 1960s, Ba-based ferroelectrics with Bi-layered structure, $BaBi_2Ta_2O_9$ (BBT) and $BaBi_2Nb_2O_9$ (BBN) were reported by Smolenskii et al. [9, 10] Sr-based layered perovskites, $SrBi_2Ta_2O_9$ (SBT) and $SrBi_2Nb_2O_9$ (SBN), are currently the major candidates for the new generation of non-volatile ferroelectric memories [11] in comparison to $BaBi_2Ta_2O_9$ (BBT), $BaBi_2Nb_2O_9$ (BBN), $CaBi_2Ta_2O_9$ (CBT), and $CaBi_2Nb_2O_9$ (CBN) [12–17].

Kartik and Verma have substituted Nb^{5+} with vanadium in $BaBi_2Nb_2O_9$ ceramics and found a significant enhancement in dielectric and ferroelectric properties [18]. Recently the same group has substituted Ba^{2+} by La^{3+} in $BaBi_2Nb_2O_9$ ceramics and found an increased

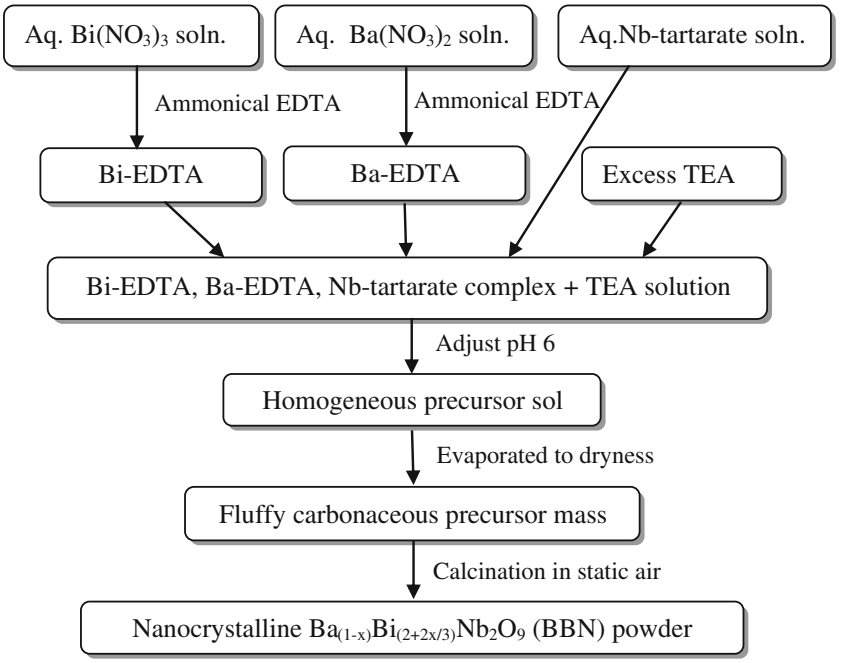

Fig. 1 Schematic representation of the precursor solution method for the synthesis of $Ba_{(1-x)}Bi_{(2+2x/3)}Nb_2O_9$ powders

diffuseness in its dielectric behavior [19]. Partial substitution of strontium ions by small size bismuth ions would increase the Curie temperature and improve the dielectric properties in both strontium bismuth tantalate, $SrBi_2Ta_2O_9$ (SBT) [20–23] and SBN [7, 24, 25] within the perovskite-like units. Park et al. have shown that the ferroelectric transition temperature (T_C) decreased with Ba^{2+} and Pb^{2+} ions but increased with Ca^{2+} ion which substitutes the 12-coordinated Sr^{2+} site, while with trivalent Bi^{3+} and La^{3+} ions, T_C increased with Bi^{3+} ion but much decreased with La^{3+} ion [26]. In these respect Ba-based counterparts; the influence of substitution by Bi^{3+} is of great interest; the synthesis has very limited reports using non-conventional techniques other than conventional solid-state method [27–30].

The phase formation temperature, chemical homogeneity, phase purity and electrical properties of multicomponent electroceramic materials like BBN, SBN, and SBT are highly dependent on the cation homogeneity in the oxide precursor [31]. In this respect the sol–gel synthesis [32, 33] and the Pechini-type polymerizable complex (PC) [34] are extremely useful. Unfortunately, the nonaqueous based solution methods (i.e. the alkoxide based solution methods using organic solvents) [35] experience hindrance in the synthesis of ceramics that contain niobium (V) ions because of the cost, and moisture sensitivity of the starting materials (such as niobium ethoxide and other alkoxides). On the other hand, the alternative aqueous based chemical processes get complicated due to scarcity of water-soluble salts of niobium and easy hydrolysis of the available ones (such as $NbCl_5$).

In the present work, we report the use of water soluble, coordinated complex of niobium-tartarate as a starting material for the preparation of nanocrystalline $Ba_{(1-x)}Bi_{(2+2x/3)}Nb_2O_9$ (x=0.0, 0.1, 0.2, 0.3, 0.4) powders through an aqueous based chemical process. Niobium-tartarate is stable in aqueous medium and is appropriate for the preparation of multi-component oxide systems comprising Nb(V) ions. The route involves the complete dehydration of an aqueous precursor solution that have the constituent metal ions in solution through formation of coordinated complexes

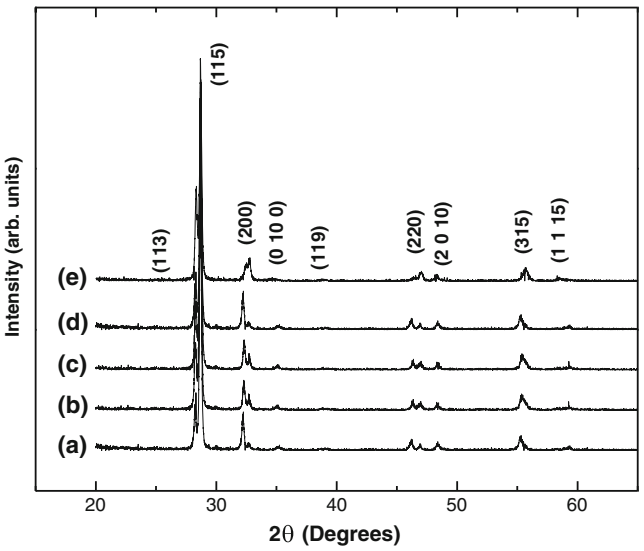

Fig. 2 X-ray diffraction pattern of BBN, (**a**) x=0.0, (**b**) x=0.1, (**c**) x=0.2, (**d**) x=0.3, and (**e**) x=0.4 ceramics powders calcined at their respective phase formation temperatures

Table 1 Compositions, phase formation temperature, crystallite size, particle size, grain size and relative density of BBN ceramics

Sample	Phase formation Temperature	Crystallite Size[a] (nm)	Particle Size[b] (nm)	Grain Size[c] (nm)	Relative density[d]
x=0.0	600°C–2 h	30	35	–	93%
x=0.1	600°C–2 h	35	38	240	91%
x=0.2	575°C–2 h	26	30	278	95%
x=0.3	550°C–2 h	24	28	–	95%
x=0.4	550°C–2 h	18	21	348	96%

[a] Average crystallite sizes for the samples heat-treated at their phase formation temperature were calculated from XRD peak broadening using the Debye-Scherrer's equation [41].

[b] Average particle sizes were calculated by the software "UTHSA" image tool (version 3.00; developed by Wilcox, Dove, McDavid, and Greer, The University of Texas Health Science Center in San Antonio, USA) from the TEM micrographs.

[c] Average grain sizes were calculated from the SEM micrographs by the same software as was used for calculating particle size.

[d] The relative density was calculated using the formula, (Experimental density/Theoretical density) × 100. The experimental densities of the sintered pellets were determined by liquid displacement using a pycnometer and xylene, as the liquid media. The density values were calculated after sintering each sample at temperature 900°C for 4 h.

with readily available, inexpensive compounds, such as, tartaric acid, ethylenediaminetetracetic acid (EDTA) and triethanolamine (TEA). Another motivation of our work was to characterize the materials as well as to study the effect of Bi^{3+} doping on structural, microstructural, dielectric and impedance characteristics of BBN ceramics.

2 Experimental

$Ba_{(1-x)}Bi_{(2+2x/3)}Nb_2O_9$ [x=0.0, 0.1. 0.2, 0.3, 0.4] was prepared by chemical solution decomposition method [36–39] using $Ba(NO_3)_2$ (MERCK, India. 99.99%), $Bi(NO_3)_3$, $5H_2O$ (Aldrich, 99.999%), Nb_2O_5 (Aldrich, 99.99%), TEA (triethanolamine) (MERCK, India. GR grade), EDTA (ethylenediaminetetracetic acid) HNO_3 (65%) (MERCK, India. GR grade), and NH_4OH (25%) (MERCK, India. GR grade).

For the preparation of various compositions of $Ba_{(1-x)}Bi_{(2+2x/3)}Nb_2O_9$ [x=0.0, 0.1. 0.2, 0.3, 0.4] the stock solutions of Ba-EDTA, Bi-EDTA, and Nb-tartarate complexes were prepared by the process described by Dhak et al. [38, 39]. It is to be mentioned that the synthesis procedure involved the preparation of Nb-tartarate from Nb_2O_5, precipitating the fluoride solution of Nb_2O_5 by diluted (30%) ammonium hydroxide solution. As mentioned in ref. [38] and [39], the Nb-hydroxide precipitate was washed thoroughly by 5% ammonium hydroxide

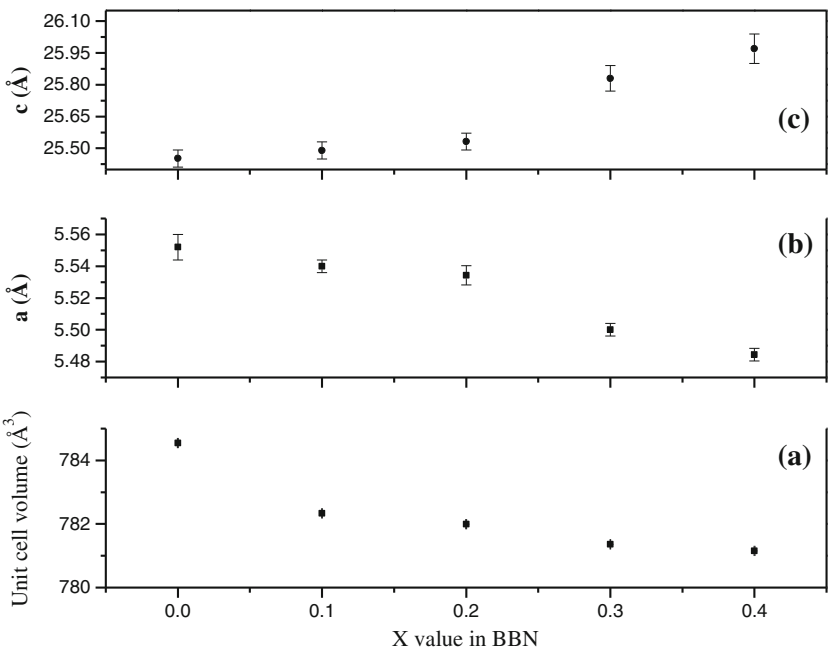

Fig. 3 Lattice constants and unit-cell volumes as a function of x in BBN, (**a**) unit-cell volume; (**b**) Lattice constant a, and (**c**) lattice constant c calculated from XRD obtained after calcining at their phase formation temperatures

solution to make sure no fluoride is present in the precipitate. The filtered solution and the precipitate were tested for flouride by spot test [40] and washing was continued until no fluoride was detected. The respective stock solutions were taken in accordance with the desired stoichiometry, and mixed together. As shown in Fig. 1, the precursor solution was subsequently obtained by adding TEA, which acts as a complexing agent [36] to the resultant mixture of the metal ion complexes. To avoid any chances of precipitation of the metal ions from the precursor solution, the amount of TEA added was always kept in excess (i.e., 3 mol ratios with respect to per mole of the total metal ions) for the required stoichiometry and the pH of the solution mixture was maintained at 6. The entire precursor solution was then rapidly evaporated by heating at ~200°C, complete dehydration of the precursor solution

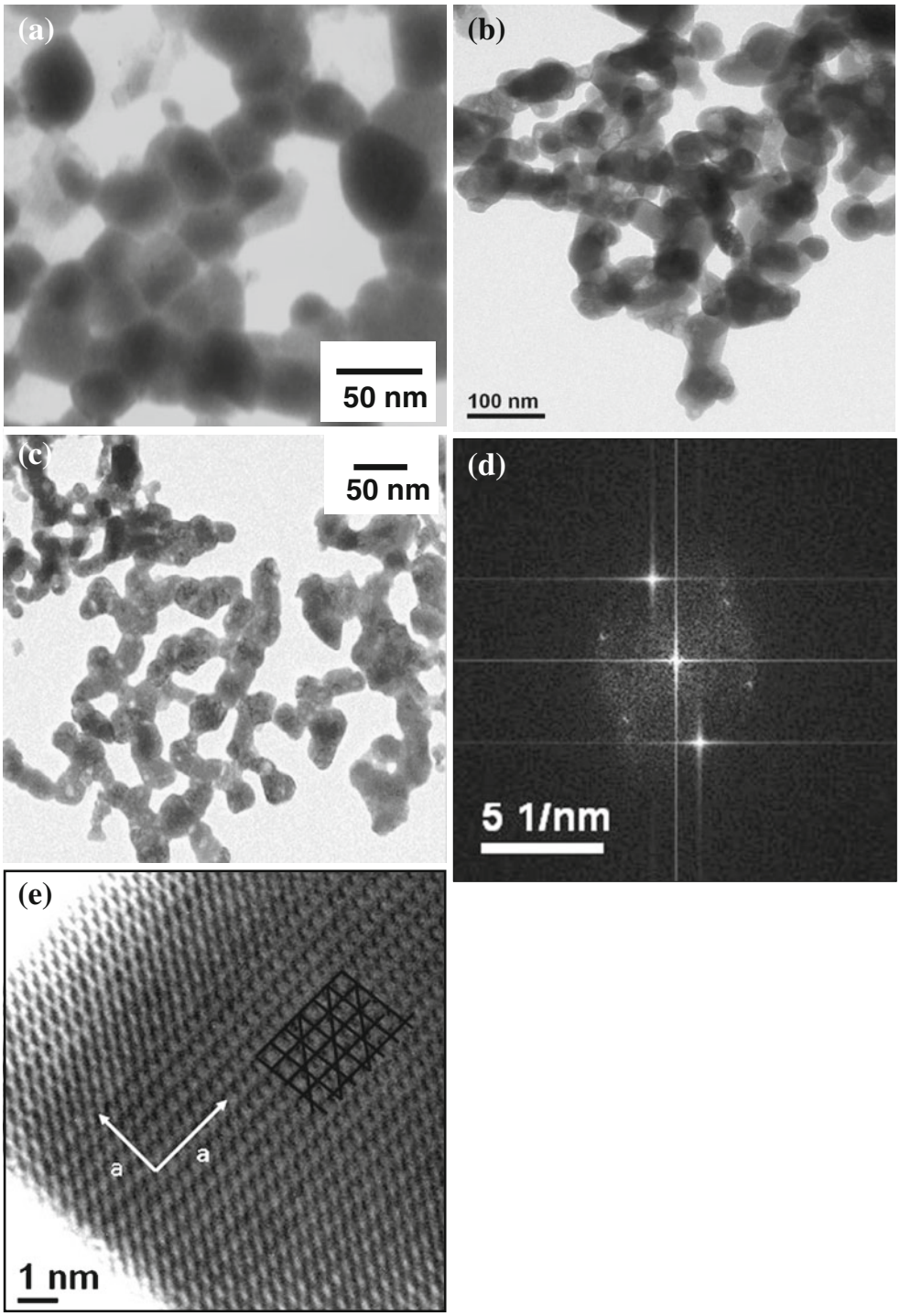

Fig. 4 Bright Field (BF) TEM of BBN (**a**) x=0.0, (**b**) x=0.2, (**c**) x=0.4, (**d**) SAED (selected area electron diffraction) pattern of BBN X=0.0 and (**e**) High resolution TEM image of BBN X=0.2

was accompanied by the decomposition of the metal complexes followed by the generation of a voluminous, carbonaceous, mesoporous precursor mass, which was ground to fine powder and subsequently calcined at different temperatures for 2 h to result in the nano-sized BBN powders. Our group has discussed the details of the mechanism of solution decomposition method using TEA in a recent communication [38].

3 Characterizations

3.1 Sample characterization

The precursor powders were heated in static air in a programmable furnace (Lenton furnace, Welland Industrial Estate, England) at a heating rate of 10°C/min in order to obtain polycrystalline BBN powder. XRD (Model: Philips PW1710 diffractometer) was used to determine the formation of the desired layered perovskite phase, for the powders. The XRD spectrum of Si crystal was used as a standard to calibrate the scanning angles. CuKα (λ=1.5418 Å) was used as target material in a wide range of Bragg angles 2θ ($20° \leq 2\theta \leq 80°$). The lattice planes were chosen for the lattice constant calculation. The fine structure of the prepared powders was analyzed by the transmission electron microscope, TEM (Model: TM-300, Philips). The sample was prepared by sonnicating a pinch of the sample for half an hour using acetone as dispersing solvent and then was taken on a carbon coated (50 nm thickness) copper grid of 300 mesh. The as-prepared powder was mixed with one drop of 1 wt% solution of polyvinyl alcohol and uniaxially pressed at room temperature for 1 min at the pressure 190 MPa. The sintering of the pressed pellets was done with the help of the same furnace, which was used for the phase formation of the precursor powders. The density of the sintered pellets was measured by pycnometer by Archimedes principle using xylene as the solvent, the density of which is 0.87 gcm^{-3}. Surface morphology of the sintered sample was checked by scanning electron microscopy (SEM) (Model JSM–5800, Japan).

3.2 Dielectric constant measurements

The electrical measurements were done on the polished pellet samples as a function of frequency at various temperatures (25 to 450°C), using an LCR meter (HIOKI, model 3532, Japan). For this purpose the sintered ceramic pellets were polished to have flat and parallel surfaces. The thickness and area of the samples were about 2.5 mm and 100 mm^2, respectively. The polished surfaces of the sample pellets were electroded by silver paste on both sides, and cured at 300°C for 2 h. A constant heating rate of 1°C/min was maintained for electrical property measurements.

4 Results and discussions

4.1 Formation of single-phase layered perovskite

During the preparation, a black fluffy mass was formed which occupies large volumes. As the calcination temperature increases, the black mass turns to yellowish in color with the removal of carbon. At higher temperatures of calcinations, no carbon was found to present. The phase formation temperatures were detected from the XRD spectra obtained at different calcination temperatures ranging from 500 to 800°C for 2 h in static air. The XRD pattern of BBN powder when calcined at 600°C indicated the phase pure BBN tetragonal structure and the entire *d*-lines pattern match with reported values [27]. The XRD patterns for all compositions are shown in Fig. 2, calcined at their phase formation temperature as summarized in Table 1. The other possible phases e.g., Bi_2O_3, BaO, or Nb_2O_5 etc. have been checked for all the sample compositions studied from standard JCPDS data file. However, it was confirmed that no other phase was identified from the XRD plots obtained from Philips PW1710 diffratometer. It was noticed that at higher concentration of bismuth doping leads to form the pure layered perovskite BBN phase at an early heat-treatment temperature. BBN with x=0.4 was found to form its layered perovskite phase only at 550°C temperature as shown in Fig. 2(e). It may be due to the fact

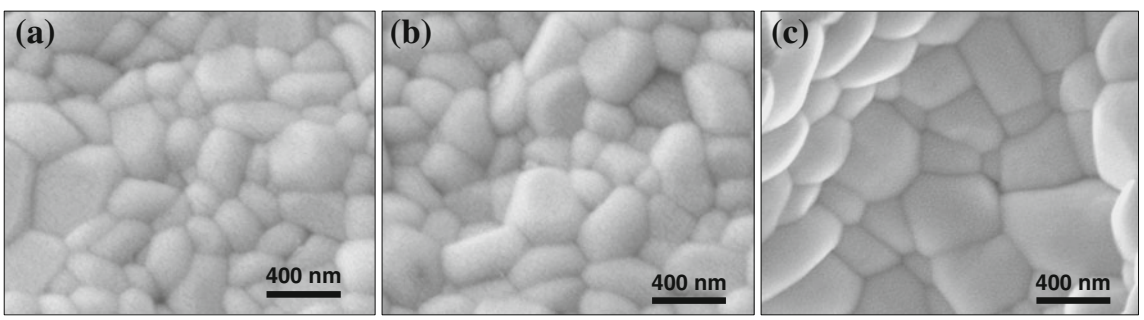

Fig. 5 SEM micrograph of the BBN compound [(**a**) x=0.1, (**b**) x=0.2, & (**c**) x=0.4] sintered at 900°C for 4 h

that the higher content of Bi with lower melting point helped to form the pure layered perovskite phase. Average crystallite sizes for the samples heat-treated at their phase formation temperature were calculated from XRD peak broadening using the Debye-Scherrer's equation [41]. In the calculation of the crystallite size, some errors may arise due to strain effect and instrumental error [42], which were corrected and summarized in Table 1. The minimum crystallite size was calculated to be 18 nm for the sample BBN x=0.4 heat-treated at 550°C for 2 h, while the maximum crystallite size was calculated to be 35 nm for the sample BBN x=0.1 heat-treated at the phase formation temperature at 600°C for 2 h.

The refined lattice constants and single unit cell volume, calculated from the XRD spectra are plotted as a function of x in BBN (Fig. 3). The lattice constant, 'a', remains almost unchanged with slight decrease with increasing x values in BBN (Fig. 3(b)) and lattice constant 'c', showed an increasing tendency with increasing bismuth concentration (Fig. 3(c)). It was noticed that the unit cell-volume attained a minimum value at the Bi doping level of 26.7 at.% (BBN x=0.4) among all investigated composition as shown in Fig. 3(a). This lowering of unit cell volume can be explained by the increasing structural constraint induced by the $[Bi_2O_2]^{2+}$ interlayer between the perovskite like units. Literature review showed that the substitution of large size Ba^{2+} ($r_{Ba}{}^{2+}$=1.75 Å) by small size Bi^{3+} ($r_{Bi}{}^{3+}$=1.34 Å) [43] lead to increase the T_m values [44, 45]. Besides that the substitution of Ba^{2+} by Bi^{3+} leads to an inhomogeneous distribution of substitution ions and local charge imbalance in a layered structure [30] which is expected to exhibit relaxor behavior of the materials.

4.2 Fine structure

The bright field TEM (Fig. 4(a), (b), and (c)) for various compositions of BBN were taken after calcinations of the precursor powders at 600°C. The bright field TEM micrographs represented the basic powder morphology in the sample, where the smallest visible isolated spot can be identified with particle/crystallite agglomerates.

The average particle diameters lay in the range of 21–38 nm (Table 1), which is in close agreement with the crystallite size obtained from XRD after corrections, is much smaller than those reported for the powders prepared through the other synthesis methods [14–16]. The corresponding selected area electron diffraction pattern of the sample BBN x=0.0 showed distinct spots, characteristic of an assembly of nano-crystallites as shown in Fig. 4(d). The image in Fig. 4(d) indicates the exact focusing of the camera of the TEM instrument. Figure 4(e) shows the high resolution TEM image of BBN, x=0.2. This lattice agrees well with the structure of the perovskite layer [46]. It is

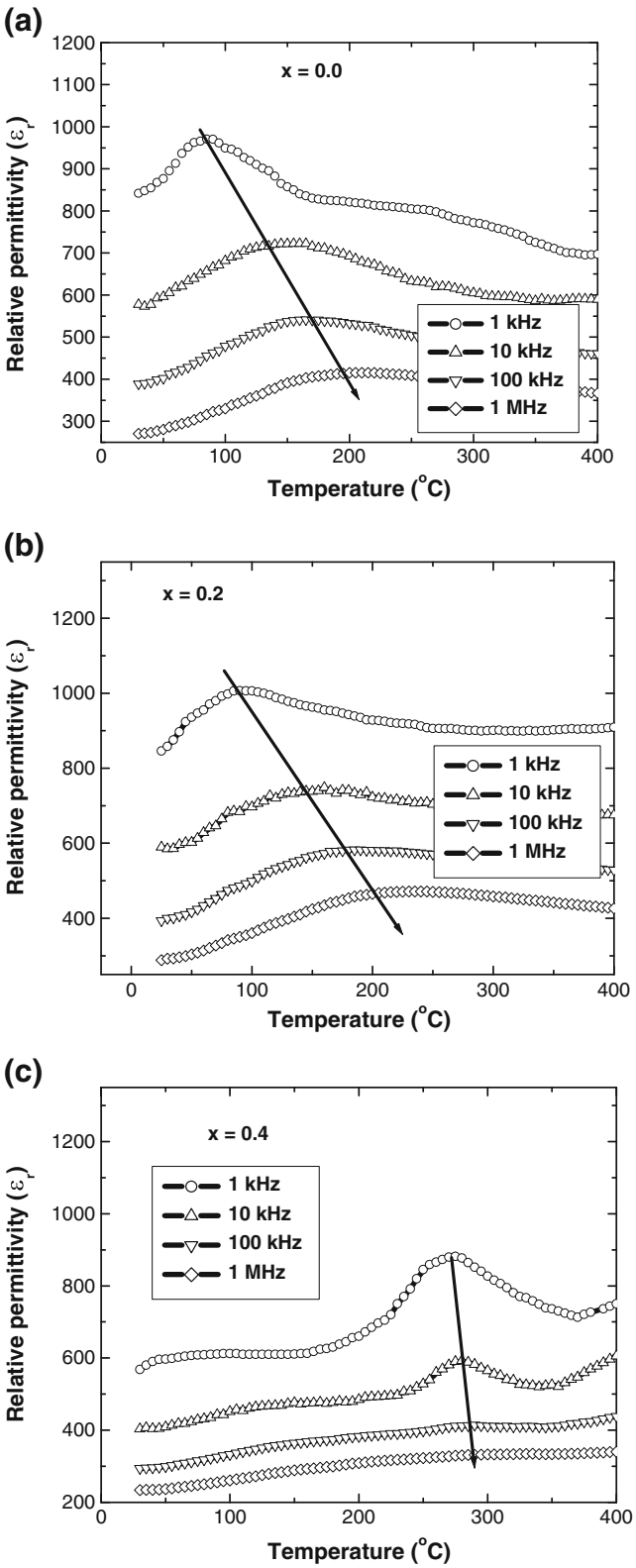

Fig. 6 Relative permittivity vs temperature at different frequencies for (**a**) BBN x=0.0, (**b**) BBN x=0.2 and (**c**) BBN x=0.4

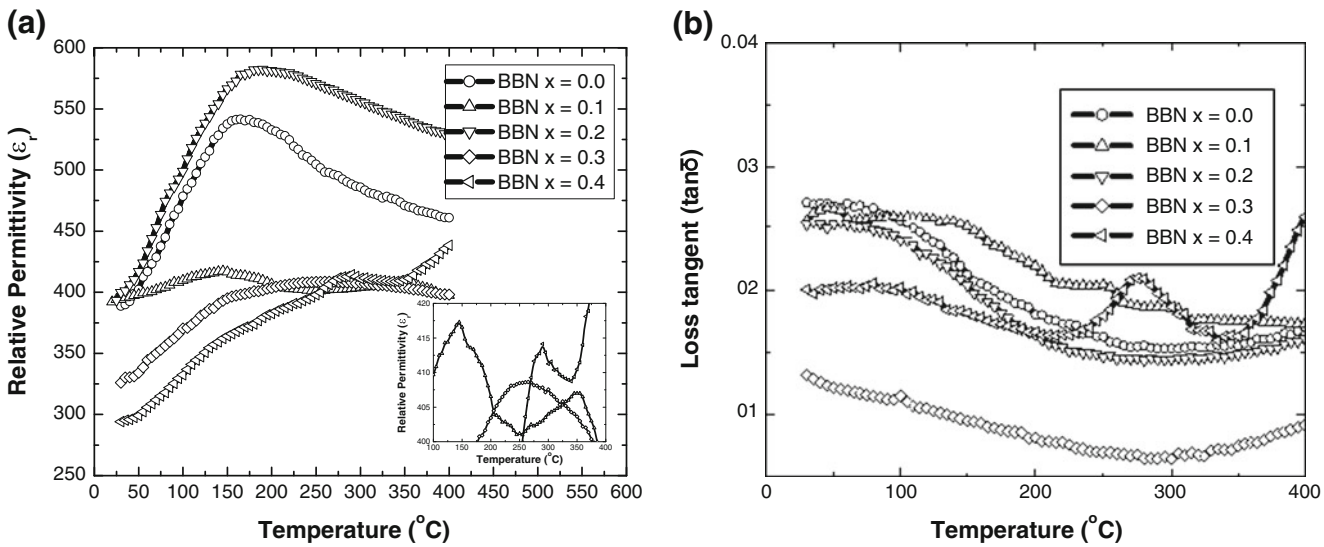

Fig. 7 Comparison of (**a**) permittivity and (**b**) loss as a function of temperature at 100 kHz for different compositions of BBN. Inset (**a**) is showing the ε_{max} for BBN x=0.1, 0.3, and 0.4

noteworthy that the uniform and clear image was observed throughout the crystallites. This appearance is very different from most of the ceramic materials, where the images are modulated due to a change in either sample thickness (in case of film) or non-uniformity. The clear image throughout the sample may be the consequence of its uniform nature.

4.3 Sintering behavior and microstructure

The sintering processes were used to prepare samples for characterizations of microstructure and property after making the pellet from the calcined powders at a uniaxial pressure 190 MPa at room temperature. The pressed pellets were subjected to the conventional solid state sintering process in static air at 900°C for 4 h. The densities of the sintered pellets were determined by liquid displacement using a pycnometer, xylene, as the liquid media. The average density obtained for pure BBN was 93% of the theoretical value, whereas 96% of theoretical density was obtained for BBN x=0.4 as reflected in the SEM images in Fig. 5(a) and (c) respectively. All other sample densities (relative) and the grain sizes are summarized in Table 1. One of the reasons for this high density with increasing doping concentration is that the addition of low melting Bi_2O_3 [43] promotes the formation of a low melting phase at the grain boundaries and facilitates the easy rotation of the grains to attain their normal growth habit during sintering. The liquid phase would effectively increase the diffusion distance between the grains, resulting a dense ceramics. The highest grain size with high density is obtained for BBN x=0.4 which is rich in Bi^{3+} content as shown in Fig. 5(c). The homogeneity and phase purity after this sintering step of the samples were checked by XRD peak from 20 to 80°. Compositional analysis (atomic ratio) obtained by EDX (energy dispersive X-ray) study of the sintered ceramics was also checked with satisfactory results.

4.4 Dielectric property

The variation of relative permittivity vs temperature at various frequencies (1 kHz, 10 kHz, 100 kHz, and 1 MHz) is shown in Fig. 6(a), (b), and (c) as few representatives for BBN x=0.0, BBN x=0.1, and BBN x=0.4 respectively. Figure 6(a) and (b) clearly show the shifts of T_m (the temperature of permittivity maxima) towards higher values on increasing frequencies. This is a clear indication of relaxor behavior of the materials. Figure (c) shows much less shifting of permittivity maxima towards higher tem-

Table 2 Permittivity (1 MHz) values at T_m and at room temperature

Sample	T_m (°C)	Relative Permittivity (100 kHz) at T_m (°C)	Relative Permittivity (100 kHz) at r.t. (25°C)
BBN x=0.0	165	540	388
BBN x=0.1	150	420	394
BBN x=0.2	185	583	400
BBN x=0.3	240	409	330
BBN x=0.4	290	418	300

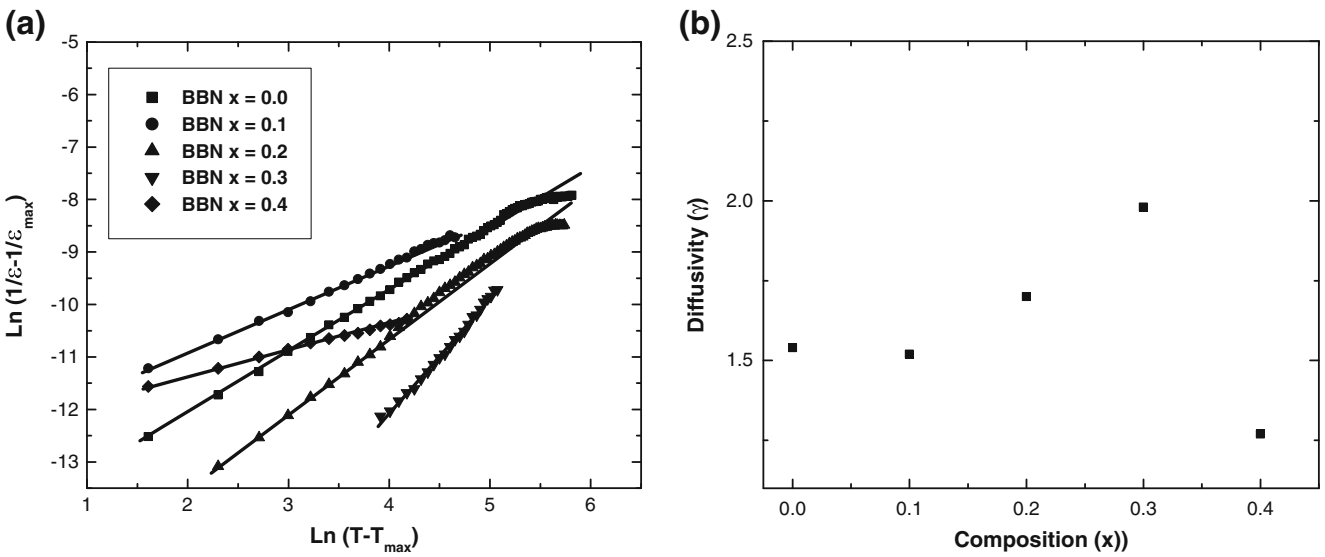

Fig. 8 Variation of (**a**) $\ln(1/\varepsilon-1/\varepsilon_{max})$ with $\ln(T-T_m)$ and (**b**) variation of γ with doping concentration at 100 kHz

perature with increasing frequencies thus less relaxor in this context for BBN x=0.4. Besides the relaxor property, the transition is quite broad which is known as diffused phase transition is also observed for all the samples as shown in Fig. 6. The rate of fall of relative permittivity was not same for all the compositions. The different dielectric dispersions for these samples may be due to different space charge contribution, which depends on the purity and perfection of the crystal and exhibit itself prominently at low frequencies. The increase in space charge polarization increased the value of relative permittivity and loss. The space charge polarization arises due to defects and impurities present either in the bulk or at the surface of the crystal or both [47].

For comparison, the variation of relative permittivity and loss tangent as a function of temperature measured at 100 kHz for all the compositions under study is shown in Fig. 7(a) and (b) respectively. Figure 7(a) (inset) is showing the ε_{max} for BBN x=0.1, 0.3, and 0.4 clearly. There are inconsistencies in the trends with increasing Bi content; BBN x=0.1 acts more like BBN x=0.3 and BBN x=0.4 while BBN x=0.2 acts more like pure BBN x=0.0. This is may be due to the structural disimilarities arising out of increasing Bi content in BBN. Table 2 lists the T_m (the temperature corresponding to first highest relative permittivity) and relative permittivity values at T_m (ε_m) for all the compositions. It has been observed as shown in Fig. 7(a) that the temperature of relative permittivity maximum shifts towards higher temperatures with increase in bismuth content. The T_m values were observed to be 165°C, 150°C, 185°C, 240°C, and 290°C respectively for BBN, x=0.0, 0.1, 0.2, 0.3, 0.4 respectively. The same figure of comparison has been reported for the analogous composition. The permittivity values both at room temperature (Fig. 6) and at the temperature of maximum relative permittivity (T_m) for all frequencies were observed to be maximum at the doping level of BBN x=0.2, as listed in Table 2. The value of ε_m (i. e., at T_m) increases from 542 for pure BBN to 583 for the composition corresponding to x=0.2. The non-stoichiometric $Sr_{1-X}Bi_{2+2X/3}Ta_2O_9$ ceramics prepared from sol–gel method by Jain et al. showed the phase transition temperature at 378°C and 455°C and maximum permittivity of 810 and 1230, respectively, for X=0.15 and 0.30 [22]. Recently Sridarane et al., and Kalaiselvi et al., reported higher Curie temperature and enhanced permittivity at the transition temperature for $Sr_{1+X}Bi_{2+(2/3)X}(V_XTa_{1-X})_2O_9$ [X=0.1 and 0.2] [48] and $Sr_{1+X}Bi_{2+(2/3)X}(V_XTa_{1-X})_2O_9$ [X=0.1 and 0.2] [23] respectively. The previous reports on the analogous series of $A_{1-x}Bi_{2+y}Nb_2O_9$, A=Sr^{2+}, Ca^{2+} (x=0.0, 0.1, 0.2, 0.3, 0.4; y=0, 0.066, 0.133, 0.200, 0.266) [44, 49]

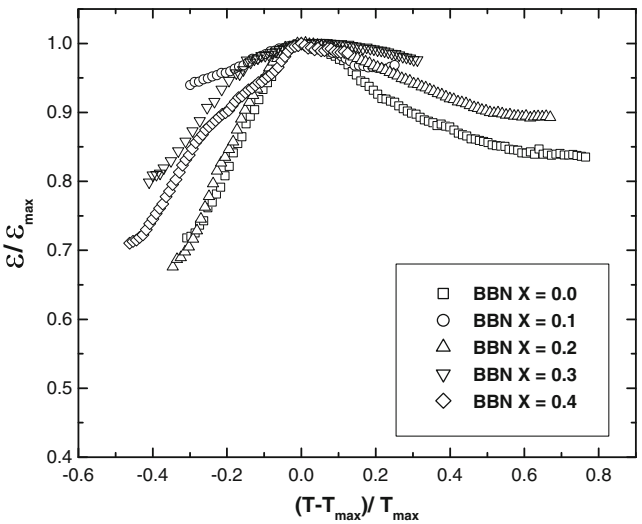

Fig. 9 Plot of normalized permittivity vs normalized temperature at 100 kHz

showed highest dielectric constant of 1040, 1610 measured at 100 kHz at T_cs, 510°C and 955°C for x=0.3 and 0.1 respectively. The loss was found to be minimum in the order of 10^{-2} for BBN x=0.3 compared to all other compositions within the temperature range investigated (Fig. 7(b)). At higher temperature (>250°C) the loss was found to increase for the sample BBN x=0.0, and BBN x=0.1 as exhibited in Fig. 7(b), which may be caused by higher concentration of charge carriers (positive and negative vacancies) at higher temperatures.

In addition to increase in T_m and ε_m, the broadness associated with relative permittivity increase with bismuth doping. To measure the diffused phase transition (DPT) of the investigated compositions the empirical relation, which is a modified form of the Curie-Weiss law, proposed by Uchino and Nomura [50], is used to describe the variation of permittivity as function of temperature above T_m for relaxors. The relation is given by

$$\frac{1}{\varepsilon} - \frac{1}{\varepsilon_{max}} = \frac{(T - T_{max})^{\gamma}}{C} \quad (1)$$

where C and γ are constants, and ε_{max} is the maximum permittivity at the transition temperature T_{max}. The constant γ determines the diffusivity of the sample system. The limiting values 1 and 2 for γ respectively reduce the expression to the Curie-Weiss law valid for a normal and the quadratic dependence for the ideal relaxor ferroelectric. Figure 8(a) shows the plots of $\ln(1/\varepsilon - 1/\varepsilon_{max})$ vs $\ln(T-T_{max})$ at 100 kHz for various compositions, the slope of which give the values of γ, the variation of which are plotted against bismuth doping percentage in Fig. 8(b). It increases from 1.54 for pure BBN to 1.98 for the composition corresponding to x=0.3. This confirms the increase in diffuseness of the dielectric anomaly with bismuth doping. However, in case of BBN x=0.4, the diffusivity reduced to 1.27. The increase of diffuseness is most likely due to the substitution Ba^{2+} by Bi^{3+} and deliberate creation of A-site vacancies [19] which promote the chemical inhomogeneity on A-site. However the lowering of γ at BBN x=0.4 is not understood.

The normalized permittivity has been plotted against normalized temperature in Fig. 9, which facilitates an analysis of all compositions simultaneously. The shape of the maxima in Fig. 9 leads us to same conclusion that the diffuseness exhibited maximum at BBN x=0.3 compared to the other substituted compositions.

5 Conclusions

The nano-sized $Ba_{(1-x)}Bi_{(2+2x/3)}Nb_2O_9$ [x=0.0, 0.1, 0.2, 0.3, 0.4] powders have been synthesized through the pyrolysis of co-ordination compounds of metal ions. A pure perovskite phase of $BaBi_2Nb_2O_9$ formed at or above 600°C for all the composition range studied. The powder has good sinteractive properties. The use of Ba-EDTA, Bi-EDTA and Nb-tartarate has been proved very effective for affording a means towards an environmentally friendly and inexpensive aqueous synthesis of the ferroelectric perovskites $Ba_{(1-x)}Bi_{(2+2x/3)}Nb_2O_9$ at reduced temperatures (600°C). The sintered pellets exhibited a room-temperature relative permittivity of about 400 with a loss of 0.01 at a frequency of 100 kHz for BBN x=0.2 ceramics. The relative permittivities at room temperature and at T_m were found to increase with increasing bismuth substitution and reached a maximum at the substitution level of BBN x=0.2. The ferroelectric phase transition was found to be diffused in the frequency range studied and the diffusivity (γ) reached to maximum of 1.98 at the doping level of BBN x=0.3.

Acknowledgement Authors thank Council of Scientific and Industrial Research and Department of Science and Technology, India, for financial support.

References

1. C.A.P. de Araujo, L.D. Mc Millan, J.D. Cuchiaro, M.C. Scott, J.F. Scott, Nature, London **374**, 627–629 (1995)
2. D.P. Vijay, S.B. Desu, J Electrochem Soc **140**, 2640–2645 (1993)
3. B. Aurivillius, Ark Kemi **5**, 39–47 (1952)
4. K. Amanuma, T. Hase, Y. Miyasaka, Appl Phys Lett **66**, 221–233 (1995)
5. T.C. Chen, T.K. Li, X.B. Zhang, S.B. Desu, J Mater Res **12**, 2165–2174 (1997)
6. E.C. Subbarao, Phys Rev **122**, 804–807 (1961)
7. J.F. Scott, C.A.P. de Araujo, Science **246**, 1400–1405 (1989)
8. S.E. Cummins, L.E. Cross, J Appl Phys **39**, 2268–2274 (1968)
9. G.A. Smolenskii, A.I. Agranovskaya, S.N. Popov, V.A. Isupov, Soviet Phys-Tech Phys **3**, 1981–1982 (1958)
10. G.A. Smolenskii, V.A. Bokov, V.A. Isupov, N.N. Krainik, R.E. Pasynkov, A.I. Sokolov, N.K. Yushin, *Ferroelectrics and related phenomena* (Gordon and Breach, New York, 1981)
11. J.F. Scott, Ferroelectrics Rev **1**, 1–129 (1998)
12. Y. Shimakawa, Y. Kubo, Y. Nakagawa, T. Kamiyama, H. Asano, F. Izumi, Appl Phys Lett **74**, 1904–1906 (1999)
13. S.R. Dhage, Y. Khollam, S.B. Dhespande, V. Ravi, Mater Res Bull **38**, 1601–1605 (2003)
14. A. Bencan, P. Boullay, J.P. Mercurio, Solid State Sci **6**, 547–551 (2004)
15. S.P. Gaikwad, V. Samuel, R. Pasricha, V. Ravi, Mater Lett **58**, 3729–3731 (2004)
16. A. Laha, S.B. Krupanidhi, Appl Phys Lett **77**, 3818–3820 (2000)
17. A. Laha, S.B. Krupanidhi, J Appl Phys **92**, 415–420 (2002)
18. C. Kartik, K.B.R. Verma, Mater Sci Eng B **129**, 245–250 (2006)
19. C. Kartik, K.B.R. Verma, M. Maglione, J. Etourneau, J Appl Phys **101**, 014106/1–014106/6 (2007)
20. J.S. Kim, C. Cheon, H.S. Shim, C.H. Lee, J Eur Ceram Soc **21**, 1295–1298 (2001)
21. A.B. Panda, A. Pathak, M. Nandagoswami, P. Pramanik, Mater Sci Eng B **97**, 275–282 (2003)
22. R. Jain, V. Gupta, A. Mansingh, K. Sreenivas, Mater Sci Eng B **112**, 54–58 (2004)

23. B.J. Kalaiselvi, R. Sridarane, R. Murugan, Ceram Int **32**, 467–470 (2006)
24. H. Tsai, P. Lin, T. Tseng, Appl Phys Lett **72**, 1787–1789 (1998)
25. E.C. Subbarao, J Chem Phys **34**, 695–696 (1961)
26. J.A. Cho, S.E. Park, T.K. Song, M.H. Kim, H.S. Lee, S.S. Kim, J Electroceram **13**, 515–518 (2004)
27. B.J. Isamunandar, J. Kennedy, Mater Chem **9**, 541–544 (1999)
28. M.E.V. Miranda, M. Costa, A.L. Avdeev, J.L. Kholkin, J. Baptista, Eur Ceram Soc **21**, 1303–1306 (2001)
29. R. Macquart, B.J. Kennedy, T. Vogt, C.J. Howard, Phys Rev B **66**, 212102/1–212102/4 (2002)
30. A.L. Kholkin, M. Avdeev, M.E.V. Costa, J.L. Baptista, Appl Phys Lett **79**, 662–664 (2001)
31. M. Kakihana, J Sol-Gel Sci Technol **6**, 7–55 (1996)
32. D.B. Beach, J.S. Morrell, Z.B. Xue, E.D. Specht, Integrat Ferroelectrics **28**, 29–36 (2000)
33. A. Pissenberger, M. Leibetseder, G. Gritzner, Adv Sci Technol **17**, 227–232 (1999)
34. A.L. Campos, T. Mazon, J.A. Varela, M.A. Zaghete, M. Cilense, Key Eng. Mater. 149–154 (189–191) (Advanced Powder Technology II), 149–154 (2001)
35. Q.F. Zhou, H.L.W. Chan, C.L. Choy, J Non-Cryst Solids **254**, 106–111 (1999)
36. A. Pathak, S. Mohapatra, S. Mohapatra, S.K. Biswas, D. Dhak, N. K. Pramanik, A. Tarafdar, P. Pramanik, Am Ceram Soc Bull **83**, 9301–9306 (2004)
37. D. Dhak, P. Pramanik, J Am Ceram Soc **89**, 1014–1021 (2006)
38. D. Dhak, S.K. Biswas, P. Pramanik, J Eur Ceram Soc **26**, 3717–3723 (2006)
39. P. Dhak, D. Dhak, P. Pramanik, Solid State Sci **10**, 1936–1946 (2008)
40. O.E.S. Godinho, Graciliano de Oliveira Neto, "A New Spot Test for Fluoride," Mikrochimica Acta [Wien], 119–122 (1974)
41. B.E. Warren, X-ray Diffraction, (Adison-Wesley, Reading, MA, 1969, pp. 253 and 258; Amorphous Materials, Wiley, New York, 1973, pp. 687 and 635; P. Scherrer, GÖttinger Nachichent 2, 1918, pp. 98
42. D. Dhak, P. Pramanik, Solid State Sci **9**, 57–64 (2007)
43. CRC Handbook of Chemistry and Physics, Internet Version 2005, David R. Lide, ed., <http://www.hbcpnetbase.com>, CRC Press, Boca Raton, FL, 2005
44. D. Dhak, P. Dhak, P. Pramanik, Appl Surface Sci **254**, 3078–3092 (2008)
45. S.E. Park, J.A. Cho, T.K. Song, M.H. Kim, S.S. Kim, H.S. Lee, J Electroceram **13**, 51 (2004)
46. Y. Ebina, T. Sasaki, M. Watanabe, Solid State Ionics **151**, 177–182 (2002)
47. R.N.P. Choudhary, B.K. Choudhary, J Mater Sci Letts **9**, 394 (1990)
48. R. Sridarane, B.J. Kalaiselvi, B. Akila, S. Subramanian, R. Murugan, Physica B **357**, 439 (2005)
49. P. Dhak, D. Dhak, K. Pramanik, P. Pramanik, Solid State Sci **10**, 1936–1946 (2008)
50. K. Uchino, S. Nomura, Ferroelectrics **44**, 55–61 (1982)